Ship Motion Control Based on AMBPS-PID Algorithm

LE WANG [ID]1, QING WU [ID]1, JIALUN LIU [ID]2,4, SHIJIE LI [ID]1, AND RUDY R. NEGENBORN [ID]3,4

[1]School of Logistics Engineering, Wuhan University of Technology, Wuhan 430063, China
[2]National Engineering Research Center for Water Transport Safety, Wuhan 430063, China
[3]Department of Maritime and Transport Technology, Delft University of Technology, 2628CD Delft, The Netherlands
[4]Intelligent Transportation Systems Research Center, Wuhan University of Technology, Wuhan 430063, China

Corresponding author: Jialun Liu (jialunliu@whut.edu.cn)

ABSTRACT Intelligent motion control is one of the key technologies of ships. This paper studies the application of Adaptive Mutation Beetle Particle Swarm (AMBPS)-PID algorithm in ship motion control. Firstly, the ship MMG model is established. Then the BAS algorithm is introduced, and AMBPS algorithm is improved and designed on this basis. Secondly, ship heading and path following controllers are designed according to the algorithm, and rudder turning rate constraint is introduced to limit the rudder angle. Thirdly, through the test function effect analysis of AMBPS and other similar algorithms, the improved effect of this algorithm is verified. Finally, from manual tuning PID parameters to off-line and on-line optimizing parameters based on AMBPS algorithm, the optimal control parameters are obtained step by step, and the optimal heading and path following simulation results are achieved. Compared with the results of traditional PID, AMBPS-PID algorithm has a better adaptive control effect on ship motion control, reduces the error of manual tuning parameters and improves efficiency.

INDEX TERMS Motion control, heading control, path following, AMBPS-PID algorithm.

I. INTRODUCTION

The main problems of ship motion control are the uncertainty of ship dynamics, random environmental disturbance and inaccuracy of measurement information [1]. For these reasons, researchers have carried out various control methods to effectively reduce the impact of these reasons, such as PID (proportion, integral and derivative), fuzzy control, predictive control, sliding mode control and other basic algorithms or their improved algorithms. Among these algorithms, the PID controller is the most widely used controllers with simple and fast characteristics. It is often combined with algorithms such as predictive algorithm and fuzzy control to control ship motion [2]–[4]. But there are still some shortcomings for the PID algorithm of a complex control system. One of them is that the fixed parameters of the PID controller

The associate editor coordinating the review of this manuscript and approving it for publication was Yilun Shang [ID].

make the algorithm unable to satisfy the precise control of a time-varying system, so the relevant scholars applied the intelligent optimization algorithm to the optimization of the parameters of the PID control. For example, ant colony (AC) algorithm [5], genetic algorithm (GA) [6], [7], particle swarm optimization (PSO) algorithm [8], neural network (NN) algorithm [9]–[12] and bacterial foraging optimization (BFO) algorithm [13] are applied to modify the PID parameters to adapt to the different operating conditions of ships.

To sum up, it is a common method to optimize the parameters of the PID algorithm based on the intelligent optimization algorithm. However, the complexity of the intelligent optimization algorithm leads to a large amount of calculation and low efficiency. Beetle Antennae Search (BAS) algorithm is a kind of bionic optimization algorithm, which is proposed in 2017. It has the advantages of low computational complexity and fast speed [14]. In recent two years, the research of the BAS algorithm has developed to BAS swarm [15] or

combined with PSO to improve the efficiency and effectiveness of optimization [16], [17]. Based on this, the paper introduces the mutation factor into the control algorithm combining BAS and PSO, and then acts on the PID control. The aim is to quickly find the optimal control parameters in the control algorithm by using a new optimization algorithm instead of manual experience.

The main contributions of this article are as follows:

1) The rudder turning rate control is introduced into the motion controller to make the control results more in line with the actual ship situation.
2) Adaptive Mutation Beetle Particle Swarm (AMBPS) algorithm is designed to replace manual experience with a new optimization algorithm. It can quickly find the optimal control parameters in the control algorithm and reduce the dynamic changes of ship control. Firstly, the special parameters can be excluded by manual tuning. Then, the algorithm variables are analyzed for a single heading angle, and the optimal PID parameters under different headings are obtained.
3) In order to realize the self-adaptability and high efficiency of the algorithm, the optimal frequency of the PID parameters is simulated and analyzed. Finally, the heading angle control and path following under the optimal parameters are realized.

Following this introduction, this paper is mainly divided into six sections. Maneuvering Modeling Group (MMG) model of the ship is built in Section II. Section III describes the AMBPS algorithm. Then, the ship motion controller based on AMBPS-PID is proposed in Section IV. Section V elaborates on the simulation results and the analysis of the algorithm. Finally, this paper makes the summaries of the results and put forward to the future research targets in Section VI. Appendix A is the symbols meaning table, and Appendix B is the comparison of testing results of basic AMBPS algorithm and other algorithms.

II. MATHEMATICAL MODELING MODEL OF A SHIP

The accuracy of the ship model affects the accuracy of motion control. Generally, ship motion models can be divided into two categories, one is the hydrodynamic model, and the other is the responsive model. The hydrodynamic model is usually divided into the Abkowitz model and the MMG model [18]. This paper chooses the MMG model because it emphasizes the physical meaning of each hydrodynamic derivative, and takes into account the interaction between ship, propeller and rudder.

The space-fixed coordinate system $o_0 - x_0 y_0 z_0$ and the moving ship fixed coordinate system $o - xyz$, shown in Fig. 1. The fixed coordinate system is set at the center of gravity of the ship.

Among them, ψ is defined as the angle between x_0 and x axes. In this paper we call it heading angle. u and v_m denote the velocity components in x and y directions respectively, and U is the total velocity. δ represents rudder angle, β is
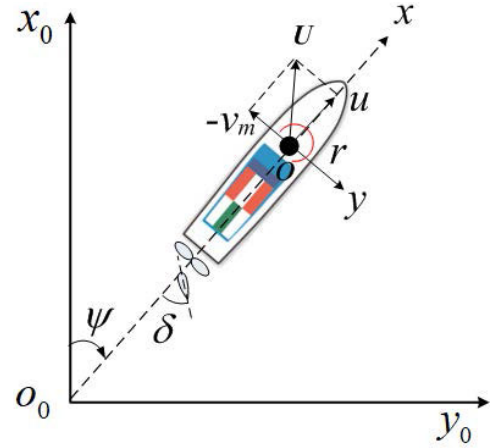

FIGURE 1. Coordinate systems.

defined as the drift angle at midship position. The maneuvering motion of a ship can be described by the MMG model as Eq. 1 [21].

$$
\left.
\begin{aligned}
X_H + \sum_{i=1}^{n_R} X_R^i + \sum_{j=1}^{n_P} X_P^j &= (m + m_x) \cdot u \\
&\quad - (m + m_y) \cdot v_m - x_G \cdot m \cdot r^2 \\
Y_H + \sum_{i=1}^{n_R} Y_R^i &= (m + m_y) \cdot \dot{v}_m \\
&\quad + (m + m_x) \cdot u \cdot r + x_G \cdot m \cdot \dot{r} \\
N_H + \sum_{i=1}^{n_R} N_R^i &= (I_{zG} + x_G^2 \cdot m + J_z) \cdot \dot{r} \\
&\quad + x_G \cdot m(\dot{v}_m + u \cdot r),
\end{aligned}
\right\}
\tag{1}
$$

where H, R and P means hull, rudder and propeller, respectively. The i and j refers to each rudder and each propeller respectively, n_R are n_p are the numbers of rudders and propellers, x_G is the longitudinal coordinate of center of gravity of ship, X, Y and N represents the longitudinal force, the transverse force and the transverse moment of the whole, respectively. The expression for the hull X_H, Y_H and N_H are as Eq. 2.

$$
\left.
\begin{aligned}
X_H &= (1/2) \cdot \rho \cdot L_{PP} \cdot d \cdot U^2 \cdot X_H'(v_m', r') \\
Y_H &= (1/2) \cdot \rho \cdot L_{PP} \cdot d \cdot U^2 \cdot Y_H'(v_m', r') \\
N_H &= (1/2) \cdot \rho \cdot L_{PP} \cdot d \cdot U^2 \cdot N_H'(v_m', r'),
\end{aligned}
\right\}
\tag{2}
$$

where the X_H' is expressed as the longitudinal force coefficient, Y_H' is the lateral force coefficient of the ship, N_H' is expressed as the yaw moment coefficient. The effective rudder forces and moments acting on the rudder are as Eq. 3.

$$
\left.
\begin{aligned}
X_R &= -(1 - t_R) \cdot F_N \cdot \sin \delta \\
Y_R &= -(1 - a_H) \cdot F_N \cdot \cos \delta \\
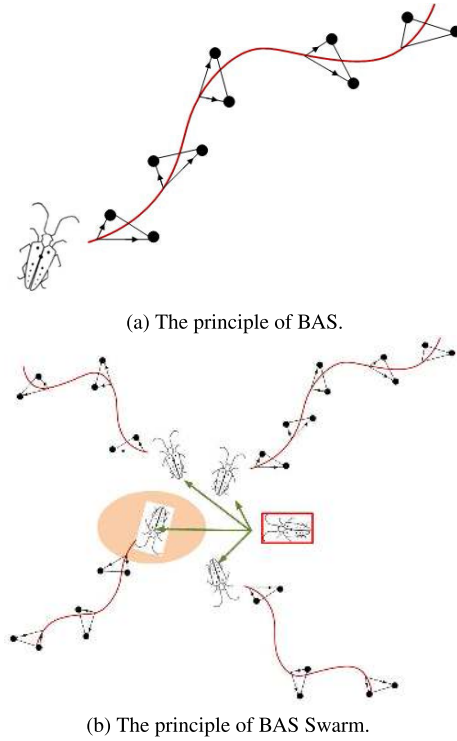N_R &= -(x_R + a_H \cdot x_H) \cdot F_N \cdot \cos \delta,
\end{aligned}
\right\}
\tag{3}
$$

(a) The principle of BAS.

(b) The principle of BAS Swarm.

FIGURE 2. BAS and BASS swarm principle.

where the F_N is the rudder normal force, a_H is the rudder force multiplier, x_R is the longitudinal coordinate of rudder position($=-0.5L_{PP}$). x_H is the longitudinal coordinate of the acting point of the additional lateral force. The surge forces due to the propeller are as Eq. 4.

$$X_P = -(1 - t_P) \cdot T \qquad (4)$$

In addition to the meanings of the symbols indicated above, the other symbols of Eq. 1, 2, 3, 4 meaning are shown in Appendix A.

III. AMBPS ALGORITHM RESEARCH

The BAS [14] is an algorithm developed for the beetle foraging principle. The basic principle of BAS is shown in Fig. 2a. Through basic research of the BAS algorithm these years, it is found that the basic BAS algorithm is easy to fall into local optimum, and the search results depend greatly on the setting of the initial position [15], [16]. Therefore, the research can be extended from an individual to a swarm, namely a BAS swarm algorithm. The principle of BAS swarm is shown in Fig. 2b. From the schematic diagram of the BAS swarm algorithm, it can be found that each beetle is equivalent to one particle, so it can be further optimized by imitating the principle of PSO.

PSO is an evolutionary algorithm that uses massless particles to simulate birds in a flock [19]. It seeks the optimal solution through cooperation and information sharing among individuals in a swarm. Similar to the PSO algorithm, a beetle can act as a particle. Each particle has only two attributes:

speed and position. Among them, speed represents the level of movement, and position represents the direction of movement. The distance and direction of beetle movement are determined by the speed and fitness of antenna detection.

Based on the above, it is assumed that there are n beetles $X = (X_1, X_2, \ldots, X_n)$ in N-dimensional space. The position of the ith beetle is expressed as $X_i = (x_{i1}, x_{i2}, \ldots, x_{iN})$ and the speed is expressed as $V_i = (v_{i1}, v_{i2}, \ldots, v_{iN})$. The individual extreme of beetles is expressed as $Pbest_i = (Pbest_{i1}, Pbest_{i2}, \ldots, Pbest_{iN})$, and the global extreme is expressed as $Gbest_i = (Gbest_{i1}, Gbest_{i2}, \ldots, Gbest_{iN})$. So the speed V_i and original position $\tilde{X}_i$ of the beetle as a particle are as Eq. 5a and Eq. 5b.

$$V_i(k) = \omega \cdot V_i(k) + c_1 \cdot r_1 \cdot (Pbest_i(k-1) - \tilde{X}_i(k-1))$$
$$+ c_2 \cdot r_2 \cdot (Gbest_i(k-1) - \tilde{X}_i(k-1)), \qquad (5a)$$
$$\tilde{X}_i(k) = \tilde{X}_i(k-1) + V_i(k), \qquad (5b)$$

Among them, ω uses "Linearly Decreasing Weight (LDW)" to adjust itself according to the number of iterations, that is $\omega(k) = \omega_{min} + (\omega_{max} - \omega_{min}) \cdot (K - k)/K$. ω_{max} and ω_{min} are the maximum and minimum weight coefficients, K is the maximum number of iterations, k is the current number of iterations.

According to the characteristics of beetle's two antennae, its movement direction can be further judged. Two N-dimensional vectors X_L and X_R are defined as the left and right antenna coordinates of beetles respectively, shown as Eq. 6. Antennae orientation can be expressed as random vector $Dir(k) = rand(N, 1)$, and Dir is normalized to $\tilde{D}(k) = Dir(k)/norm(Dir(k))$. Besides, $D_0 = L_{step}/b_2$.

$$\left.\begin{array}{l} X_{Li}(k) = \tilde{X}_i(k) + D_0 \cdot \tilde{D}(k)/2 \\ X_{Ri}(k) = \tilde{X}_i(k) - D_0 \cdot \tilde{D}(k)/2 \end{array}\right\} \qquad (6)$$

X_i represents the beetle centroid coordinates and is also the updated position coordinates of the beetle. The calculation method of X_i is shown in Eq. 7, then the initial cost value is calculated according to X_i, which is regarded as the current optimal fitness function value f_{best}.

$$X_i(k) = \tilde{X}_i(k) - L_{step} \cdot normal(X_{Li}(k) - X_{Ri}(k)) \ldots$$
$$\cdot sign(f(X_{Li}(k)) - f(X_{Ri}(k))) \qquad (7)$$

The optimal fitness function is calculated according to the updated beetle position $X_i(k)$ in each iteration cycle. Then compare and update the current best parameters $X_{best}(k)$ and f_{best} according to Eq. 8.

$$\left.\begin{array}{l} f_{best}(k) = f|_{X_i(k)} \\ X_{best}(k) = X_i(k) \end{array}\right\}, \quad f|_{X_i(k)} < f_{best} \qquad (8)$$

Update L_{step} and D_0. L_{step} and D_0 can be updated by the proportional method or other methods. If the optimal fitness value decreases gradually, only the beetle position $X_i(k)$ needs to be updated. On the contrary, the L_{step} and D_0 should be attenuated until the control is over or the optimal

fitness value set is satisfied. Because it means that the current L_{step} and D_0 can not get the optimal position, shown in Eq. 9.

$$\left.\begin{array}{l} L_{step}(k) = b_1 \cdot L_{best}(k-1) \\ D_0(k) = L_{step}(k-1)/b_2 \end{array}\right\}, \quad f|_{X_i(k)} < f_{best} \quad (9)$$

As the search proceeded, the difference between individual positions of beetles gradually decreased and the concentration degree increased. To further reduce the probability of the algorithm falling into local optimum, an adaptive mutation operator is introduced in this paper. The basic principles are as follows: Firstly, the variance of population fitness function and spatial location aggregation degree are analyzed, then the diversity of the population is increased by judging whether an adaptive mutation is needed in threshold selection, and finally, the global optimization is realized.

At the current kth iteration, the fitness function is $f_i(k) = f|_{X_i(k)}$, and the average fitness function of the population is $f_{ave}(k)$, then the fitness variance of the population is defined as Eq. 10. In this paper, $\Theta(k)$ is used to reflect the aggregation degree of a single beetle in the beetle population.

$$\Theta(k) = \sum_{i=1}^{n} \left(\frac{f_i(k) - f_{avg}(k)}{\tilde{f}(k)} \right)^2, \quad (10)$$

where, $\tilde{f}(k) = max\{max\{|f_i(k) - f_{avg}(k)|\}, 1\}, i \in [1, n]$, its function is to limit the size of $\Theta(k)$.

In addition, the degree of aggregation between beetles can also be expressed as Eq. 11 by $\tau(k)$. The larger the $\tau(k)$, the lower the probability of mutation.

$$\tau(k) = \frac{\max\limits_{1 \le i \le n}\left\{\|X_i(k) - Pbest_i(k)\|\right\}}{\max\limits_{k}\left\{\max\limits_{1 \le i \le n}\left\{\|X_i(k) - Pbest_i(k)\|\right\}\right\}} \quad (11)$$

When $\Theta(k)$ tends to zero and $\tau(k)$ decreases, the algorithm may fall into premature convergence. Define mutation probability $p_m(k)$ as Eq. 12.

$$p_m(k) = \begin{cases} e^{-\tau(k)}/5, & \Theta(k) < \Theta_0 \\ 0, & \Theta(k) \ge \Theta_0 \end{cases} \quad (12)$$

Θ_0 is a threshold set according to the actual situation, usually close to 0. According to this probability, the mutation sequence is generated and the extreme of each individual is adjusted, such as Eq. 13. Among them, p_{rand} is a random number between 0 and 1, and η is a N-dimensional random vector obeying $(0, 1)$ normal distribution.

$$Pbest_i(k) = \begin{cases} Pbest_i(k) \cdot (1 + 0.5\eta), & p_{rand}(k) < p_m(k) \\ Pbest_i(k), & p_{rand}(k) \ge p_m(k) \end{cases} \quad (13)$$

IV. DESIGN OF SHIP MOTION CONTROLLER BASED ON AMBPS-PID

A. SHIP HEADING CONTROLLER
The aim of heading control is to calculate the rudder turning rate command of each step, and then input it into the ship
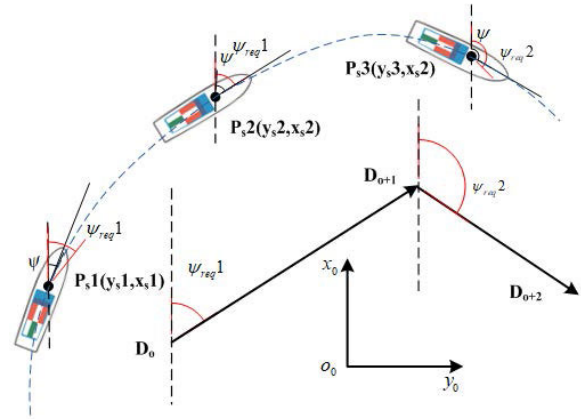

FIGURE 3. Heading tracking schematic.

motion model to get the next step heading angles, so as to gradually realize the target heading. Based on this, the control variables of heading control in this paper is $\dot{\delta}_E$ and the control output is ψ. In the $o_0 - x_0y_0z_0$ coordinate system used in this paper, Direction of vectors $\overrightarrow{D_oD_{o+1}}$ ($o = 1, 2, \ldots$) represents the target heading ψ_{req}. $P_s(y_s, x_s)$ is the current position of the ship, as shown in Fig. 3.

Heading tracking aims to make the current heading angle of the ship follow the target heading angle. The heading error ψ_{error} at t_{step}(indicated by λ) is as Eq. 14.

$$\psi_{error}(\lambda) = \psi(\lambda) - \psi_{req}(\lambda). \quad (14)$$

Based on the ψ_{error} and the basic principle of the PID algorithm, the next time step of the rudder command is shown as Eq. 15.

$$\delta_E(\lambda + 1) = K_P\psi_{error}(\lambda) + K_I \sum_{j=1}^{K} \psi_{error}(\lambda)$$
$$+ K_D(\psi_{error}(\lambda) - \psi_{error}(\lambda - 1)) \quad (15)$$

According to the type of ship, rudder angle has a range of constraints, set to $[\delta_{E_{Lmax}}, \delta_{E_{Rmax}}]$. It needs to be judged after getting the $\delta_E(\lambda + 1)$, shown as Eq. 16.

$$\delta_E(\lambda + 1) = \begin{cases} \delta_{E_{Lmax}}, & \delta_E(\lambda + 1) > \delta_{E_{Lmax}} \\ \delta_{E_{Rmax}}, & \delta_E(\lambda + 1) > \delta_{E_{Rmax}} \end{cases} \quad (16)$$

In practical applications, especially for large-scale ships, because of its huge mechanical structure, the rudder rotation has a certain speed. The rudder angle commands given by the control decision system need to be accumulated over a certain period time before they can be realized. Most of the current studies ignore the rudder turning time. It is directly considered that the rudder angle has reached the required target rudder angle in the next step, so it has a certain error compared with the actual situation. This article introduced the rudder turning rate constraint for the object(7 meters ship). It controls the rudder turning rate in each execution. Rudder turning rate control principle is as Eq. 17.

$$\dot{\delta}_E(\lambda + 1) = (\delta_E(\lambda + 1) - \delta(\lambda))/t_{step}, \quad (17)$$
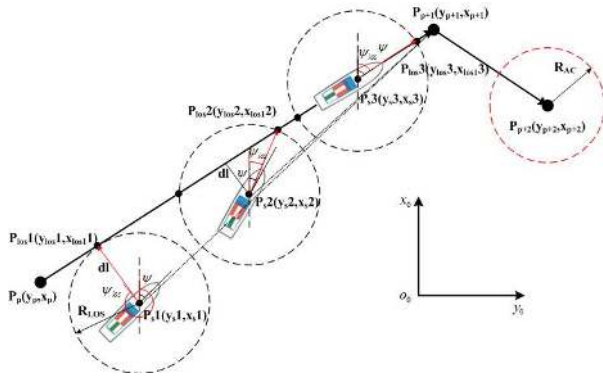
FIGURE 4. The principle of LOS navigation.

among them, t_{step} is the time step, $\dot{\delta}(\lambda + 1)$ is the next time step rudder turning rate. Besides, rudder turning rate is constrained by left and right rudder turning rate, set to $[\dot{\delta}_{ELmax}, \dot{\delta}_{ERmax}]$. The $\dot{\delta}(\lambda + 1)$ is obtained according to the constraints, shown as Eq. 18.

$$\dot{\delta}_E(\lambda + 1) = \begin{cases} \dot{\delta}_{ELmax}, & \dot{\delta}_E(\lambda + 1) > \dot{\delta}_{ELmax} \\ \dot{\delta}_{ERmax}, & \dot{\delta}_E(\lambda + 1) > \dot{\delta}_{ERmax} \end{cases} \quad (18)$$

Then the rudder angle obtained through integral after judging the rudder turning rate. It can be used on the MMG model to make a series calculation.

B. SHIP PATH FOLLOWING CONTROLLER

LOS navigation is a method to simulate the sight of experienced sailors to achieve convergence to the desired path [20]. In this paper, LOS guidance law is used to track the LOS angle, and then the track tracking results are obtained. The goal of path following is to calculate the rudder turning rate command controlled by each step and then input it into the ship motion model. Based on the principle of LOS navigation, it can gradually track the heading and then track the target path. In this paper, the control variable is $\dot{\delta}_E$ and the control output is ψ and P_s. The principle of LOS navigation is shown in Fig. 4.

As shown in the Fig. 4, path points P_p $(p = 0, 1, 2, \ldots)$ constitute the desired path, and the line between two adjacent points P_pP_{p+1} is a straight line. Among them, the straight line formed by $P_p(y_p, x_p)P_{p+1}(y_{p+1}, x_{p+1})$ is the current desired path. $P_{los}(y_{los}, x_{los})$ is the closest point between the Los circle and the next point in the intersection of the target path. ψ_{los} is defined as an angle within $0 - 360$ degrees with the northward direction as the reference point. It can be seen that no matter where the ship is currently located in $P_s(y_s, x_s)$, the solution formula of $P_{los}(\lambda)(y_{los}(\lambda), x_{los}(\lambda))$ is as Eq. 19a. Then the calculation method of $\psi_{los}(\lambda)$ is shown in Eq. 19b.

$$P_{los} = \begin{cases} \dfrac{x_{los}(\lambda) - x_p}{y_{los}(\lambda) - y_p} = \dfrac{x_{p+1} - x_p}{y_{p+1} - y_p} \\ (y_{los}(\lambda) - y_s(\lambda))^2 + (x_{los}(\lambda) - x_s(\lambda))^2 = R_{AC}^2, \end{cases} \quad (19a)$$

$$\psi_{los}(\lambda) = \arctan \frac{y_{los}(\lambda) - y_s(\lambda)}{x_{los}(\lambda) - x_s(\lambda)}, \quad (19b)$$

Besides, it can be seen from Fig. 4 that there is one or two intersection points, and there may be no real solution when the ship deviates from the desired path. To avoid this, R_{los} is usually set to ζ times of captain L_{pp}. In order to ensure the adaptability of ship path following, LOS circle is set as a dynamic circle. R_{los} can be defined as:

$$R_{los}(\lambda) = dl(\lambda) + \zeta L_{pp} \quad (20)$$

among them, the vertical distance $dl(\lambda)$ from the ship's position point to the target path is:

$$\left. \begin{array}{l} d_a = \sqrt{(y_s(\lambda) - y_{p+1})^2 + (x_s(\lambda) - x_{p+1})^2} \\ d_b = \sqrt{(y_{p+2} - y_s(\lambda))^2 + (x_{p+2} - x_s(\lambda))^2} \\ d_c = \sqrt{(y_{p+2} - y_{p+1})^2 + (x_{p+2} - x_{p+1})^2} \end{array} \right\} \quad (21a)$$

$$dl(\lambda) = \sqrt{d_a^2 - ((d_c^2 - d_b^2 + d_a^2)/(2d_c))^2} \quad (21b)$$

When the ship approaches the target point $P_{p+1}(y_{p+1}, x_{p+1})$, the target path needs to be switched from P_pP_{p+1} to $P_{p+1}P_{p+2}$. When the ship enters the acceptance circle with P_{p+1} as the center and R_{AC} as the radius, that is, $(y_s(\lambda) - y_{p+1})^2 + (x_s(\lambda) - x_{p+1})^2 \le R_{AC}^2$, the target path is switched. In order to ensure that point $P_{los}(\lambda)$ may be located at inflection point P_{p+1}, this paper defines R_{AC} as: $R_{AC} = R_{los}(\lambda)$.

Finally, let $\psi_{req} = \psi los$. Based on Section IV-A, the rudder turning rate command can be obtained to achieve path following.

C. SHIP MOTION CONTROLLER BASED ON AMBPS-PID ALGORITHM

This paper combines the AMBPS algorithm with the PID algorithm to design the ship motion controller. The flow chart of the algorithm is shown in Fig. 5. As shown in Fig. 5, the k step variable values are calculated by the $k - 1$ step variable values. In this paper, the control variables are three parameters of PID: K_P, K_I, K_D. Then the current global optimal fitness function value is judged and stored, and self-adaptively judge whether the control variables need to be mutated according to the control situation. For ship heading control and path following control, the fitness function $f(x)$ is shown in Eq. 22 and 23, respectively. As shown in Eq. 22 and 23, the fitness function is set as the tracking error of heading or path. The error judgment standard uses Root Mean Square Error(RMSE) and Mean Absolute Deviation(MAD). RMSE is used to measure the deviation between the observed value and the true value. It is very sensitive to the extremely large and very small errors in the results. Since MAD is absolutely quantized, the positive and negative phase cancellation will not occur. Therefore, the average absolute error can better reflect the actual situation of the error.

$$f_1(x) = \begin{cases} \dfrac{\sum_{k=1}^{K} |\psi_{error}|}{K}, & \text{Minimum MAD as standard.} \\ \sqrt{\dfrac{\sum_{k=1}^{K} \psi_{error}^2}{K}}, & \text{Minimum RMSE as standard.} \end{cases}$$
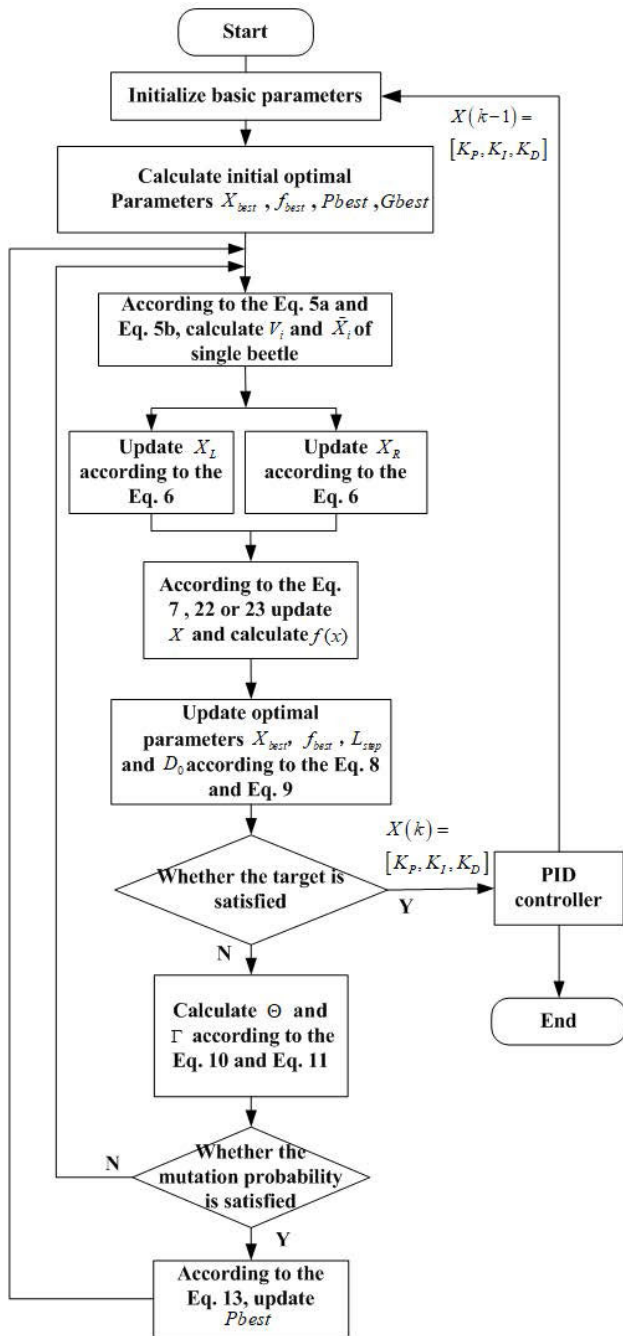
$$(22)$$

FIGURE 5. Flow charts of AMBPS-PID algorithm.

$$f_2(x) = \begin{cases} \dfrac{\sum_{k=1}^{K} |dl|}{K}, & \text{Minimum MAD as standard.} \\[4mm] \sqrt{\dfrac{\sum_{k=1}^{K} dl^2}{K}}, & \text{Minimum RMSE as standard.} \end{cases}$$

(23)

Besides, to analyze the application effect of the algorithm, the off-line and on-line controllers of ship motion are designed in this paper, as shown in Fig. 6. The off-line controller is to automatically find the most precise

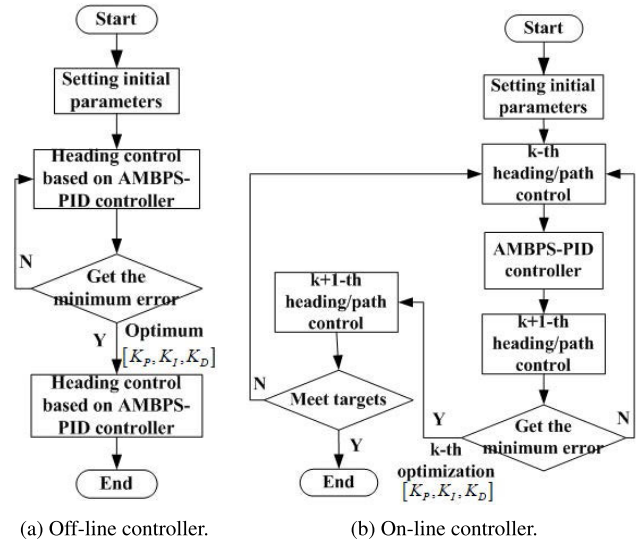(a) Off-line controller. (b) On-line controller.

FIGURE 6. Flow charts of off-line and on-line controllers.

PID parameters through multiple cycles, which is suitable for single heading control. The on-line controller is a self-adaptive controller that automatically updates and optimizes the PID parameters in a single or k steps. The aim is to obtain the optimal PID parameters in the current or future k steps.

V. SIMULATION AND COMPARISON
A. SIMULATION AND COMPARISON OF AMBPS ALGORITHM
To ensure the effectiveness of the AMBPS optimization algorithm, this paper takes six classical global optimal test functions as examples to compare and analyze the effectiveness of the AMBPS algorithm. Six classical global optimal functions have their characteristics, which can effectively test whether the algorithm can jump out of local optimum.

- The Rastrigrin function is characterized by a large number of deep local optima arranged by sinusoidal inflection points.
- The product term between variables of the Griewank function has strong interaction and is a multi-modal function.
- The Michalewicz function is a standard benchmark function with several local minimum values and plane regions.
- The Goldstein-Price function has several local minimum values.
- Ackley function is characterized by an almost flat region modulated by cosine waves forming holes or peaks, which make the surface undulate and uneven.
- The characteristic of the Schaffer function is that the local optimal value is located on the concentric circle near the global optimal value, while the global optimal value is located in a very narrow concave region.

This paper designs AMBPS to compare with BAS [14], BAS Swarm, PSO ,and BAS-PSO [16] algorithms. When the
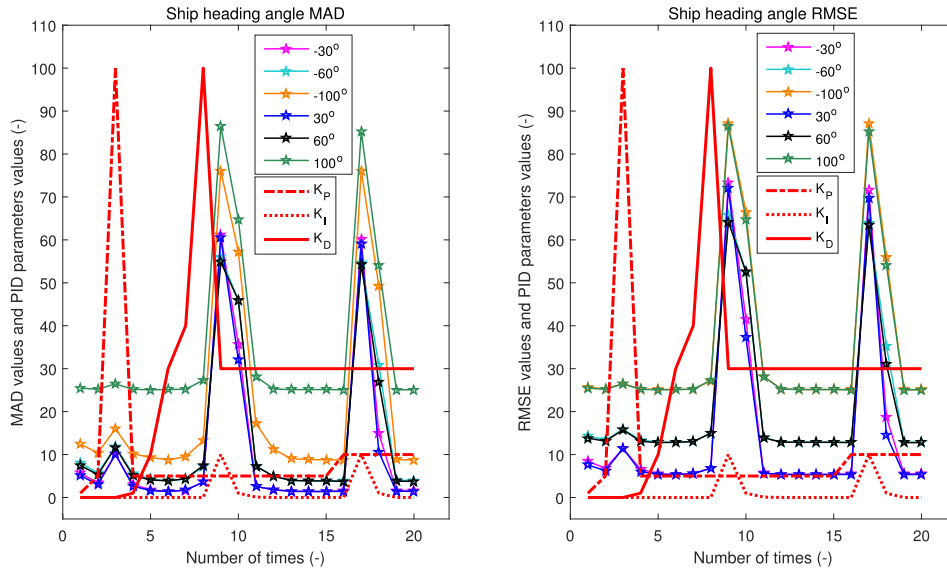
FIGURE 7. Tracking RMSE and MAD for Ship single target heading angle.

TABLE 1. Main particulars of the 7m KVLCC2 ship.

Symbols	Value	Symbols	Value
a_H	0.312	T	0.455
B_{wl}	1.1688	t_p	0.220
d	0.46	t_R	0.387
∇	3.2724	x_G	0.244
J_z'	0.011	x_H'	-0.46
L_{pp}	7.0	x_R'	-0.5
n_p	10.4	$[\delta_{Lmax}, \delta_{Rmax}]$	[-35,35]
m_x'	0.022	$[\dot\delta_{Lmax}, \dot\delta_{Rmax}]$	[-15.8,15.8]
m_y'	0.223	ρ	1025

TABLE 2. RMSE and MAD values for tracking different heading angles (Manual).

Heading	-30°	-60°	-100°	30°	60°	100°
MAD	1.3843	3.9725	8.7925	1.4023	3.8593	8.8273
RMSE	5.3569	12.8798	25.1485	5.3708	12.8540	25.1333

$Titer = 1000$ and $n = 10$, the average error of 10 times calculations and the comparison results are detailed in Appendix B. It can be seen from Appendix B that the AMBPS algorithm is more stable than other algorithms in the case of ensuring high precision, and can effectively avoid falling into local optimum. To optimize the parameters of the PID algorithm in this paper, the adaptive and stable characteristics are the preferred standard for selecting optimization algorithms. Therefore, the shortcomings of AMBAS sometimes having a slight lack of optimization speed can be ignored.

B. SIMULATION RESULTS OF THE SHIP HEADING CONTROL WITH MANUAL SEARCHING PID PARAMETERS

In this paper, the 7m KVLCC2 ship is selected as the simulation object. The basic parameters of the ship are shown in Table 1. Detailed parameters can be found in reference [21].

According to the actual ship's navigation situation, the range of the ψ in this paper is specified as $[-180°, 180°]$, and any target heading angle ψ_{req} is selected to simulate in this range. For a single heading angle, we choose $-30°, -60°, -100°, 30°, 60°, 100°$ as examples to test. Firstly, PID parameters are searched manually, and the

control errors under different parameters are obtained, as shown in Fig. 7.

In Fig. 7, the red lines represent the changes of the values of the PID parameters $[K_P, K_I, K_D]$, while the other lines represent the MAD and RMSE values with the changes of the PID parameters under the different heading angle targets. It can be concluded from Fig. 7: The change of K_I has a great influence on the error, both MAD and RMSE values. Only when K_I approaches 0, the influence on the error is extremely small, so K_I is directly set to 0 in this paper. This is the only certain PID parameter value that can be obtained by manual adjustment. Now the optimal PID parameter can be roughly obtained as $[K_P, K_I, K_D] = [5, 0, 20]$.
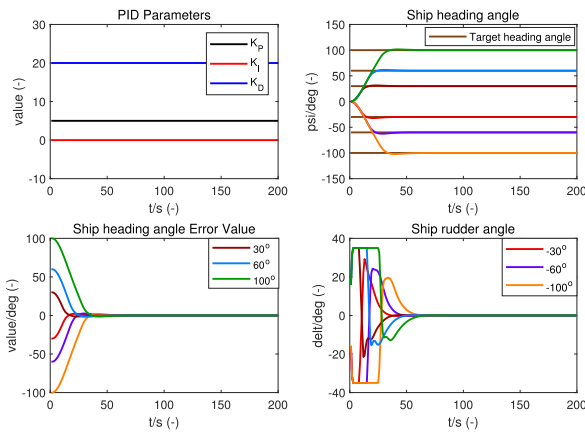
1) TRACKING A SINGLE HEADING ANGLE
Based on the manually adjusted PID parameter values $[K_P, K_I, K_D] = [5, 0, 20]$, the tracking step is set $nStep = 200$. Taking $-30°, -60°, -100°, 30°, 60°, 100°$ as an example, the tracking result is shown in Fig. 8. Fig. 8a shows the ship trajectories under different headings, and 8b shows the changes of PID parameters, the tracking heading angle, the tracking error per t_{step} and the rudder angle respectively. The heading tracking error MAD and RMSE results are shown in Table 2.

2) TRACKING TIME-VARYING HEADING ANGLES
Based on the manually adjusted PID parameter values $[K_P, K_I, K_D] = [5, 0, 20]$, the tracking step is set
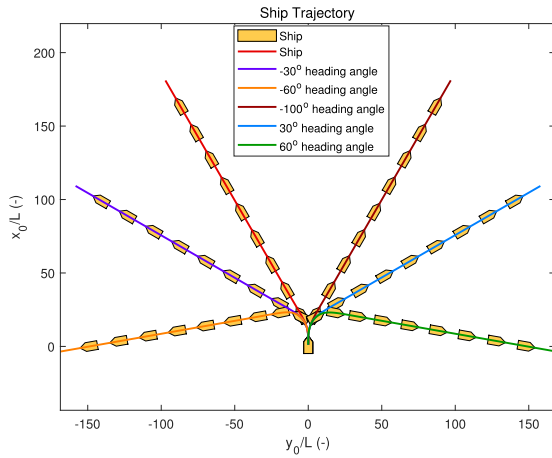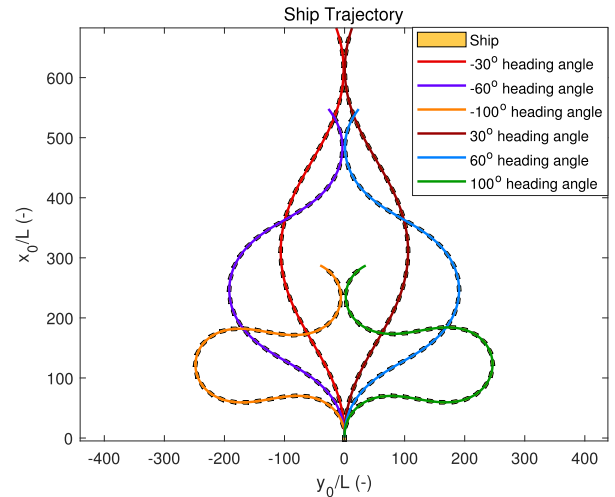
(a) Ship trajectory.

(b) Ship tracking details.

FIGURE 8. Tracking different heading angles (Manual).

TABLE 3. MAD and RMSE values for tracking time-varying heading angles ($\psi_{req} = Asin(0.01t)$, Manual).

A	-30°	-60°	-100°	30°	60°	100°
MAD	0.2135	0.4118	0.6324	0.2033	0.3911	0.5979
RMSE	0.2406	0.4637	0.7112	0.2276	0.4373	0.6672

$nStep = 700$. Similarly, the heading angle with sinusoidal function in $[-180°, 180°]$ is chosen as the target heading angle, as shown in Fig. 9. Fig. 9a shows the ship trajectories under different headings, and 9b shows the changes of PID parameters, the tracking heading angle, the tracking error and the rudder angle respectively. The MAD and RMSE for tracking time-varying heading angles are obtained, as shown in Table 3.

From the above results, it can be concluded that the manual adjustment of parameters can achieve better tracking effect, but it needs to keep trying to find the better parameters. This method is inefficient and uncertain whether it is the optimal value, which can be used for initial judgment. Especially for the parameter K_I in this paper, the optimal result can be obtained by manual adjustment.

(a) Ship trajectory.
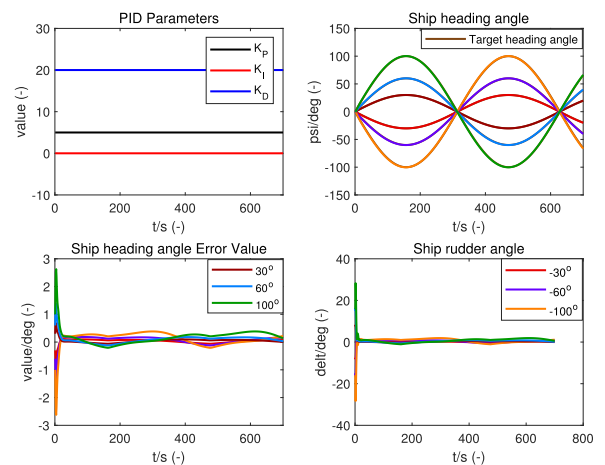
(b) Ship tracking details.

FIGURE 9. Tracking different time-varying heading angles (Manual).

C. SIMULATION RESULTS OF THE SHIP HEADING CONTROL AND PATH FOLLOWING WITH AMBPS-PID ALGORITHM

1) TRACKING A SINGLE HEADING ANGLE (OFF-LINE CONTROLLER)

The basic control parameter values of the AMBPS-PID algorithm are shown in Table 4. According to Section III, it can be found that the basic variables that may affect the results are n, L_{step}, D_0 and V_m. Using the control variable method, setting the search times $Titer = 100$. Based on the Table 4, the influence of variables is analyzed as follows.

1) With MAD optimum as the standard, the optional angle can be selected for simulation. There we choose $60°$ as an example, the tracking error and the optimal PID parameters under different variables values are obtained as shown in Table 5.

Optimum parameters are obtained from Table 5 are $n = 10$, $D_0 = 0.99$, $L_{step} = 1$, $Vm = 5$. Under the optimal control variables, any other angle can be

TABLE 4. AMBPS-PID algorithm basic parameter values.

Symbols	Value	Symbols	Value
$nStep$	200	V_m	5
$c1, c2$	2	$b1$	0.95
n	200	$b2$	0.99
N	200	L_{step}	1
K_P, K_I, K_D	0,0,0	D_0	0.99

TABLE 5. Tracking error and the optimal PID parameters under different variable values ($\psi_{req} = 60°$, minimum MAD).

n	K_P	K_I	K_D	MAD	RMSE
2	9.47886	0	37.2362	3.6496	12.8163
5	9.51667	0	40.3671	3.6462	12.8179
10	9.67247	0	41.1822	3.6459	12.8179
20	9.7174	0	41.4115	3.6459	12.8179
30	9.71773	0	41.4128	3.6459	12.8179
D_0	K_P	K_I	K_D	MAD	RMSE
0.99	9.67247	0	41.1822	3.6459	12.8179
2	9.67264	0	41.1921	3.6459	12.8179
5	9.59186	0	40.7746	3.646	12.8179
10	9.67021	0	40.9602	3.6463	12.8179
20	9.68647	0	41.2678	3.6459	12.818
L_{step}	K_P	K_I	K_D	MAD	RMSE
0.5	9.72714	0	41.4605	3.6459	12.8179
1	9.67247	0	41.1822	3.6459	12.8179
3	9.51029	0	40.3375	3.6462	12.8179
5	9.60947	0	40.8454	3.646	12.8179
10	9.72412	0	41.4308	3.6459	12.8179
V	K_P	K_I	K_D	MAD	RMSE
0.5	5.577553	0	17.9149	3.7267	12.8226
1	9.52079	0	40.3599	3.6462	12.8178
5	9.67247	0	41.1822	3.6459	12.8179
10	9.7269	0	41.2848	3.6461	12.8175
20	9.64156	0	41.0242	3.6459	12.8179

TABLE 6. Tracking different heading angle errors and PID parameters (AMBPS-PID, minimum MAD).
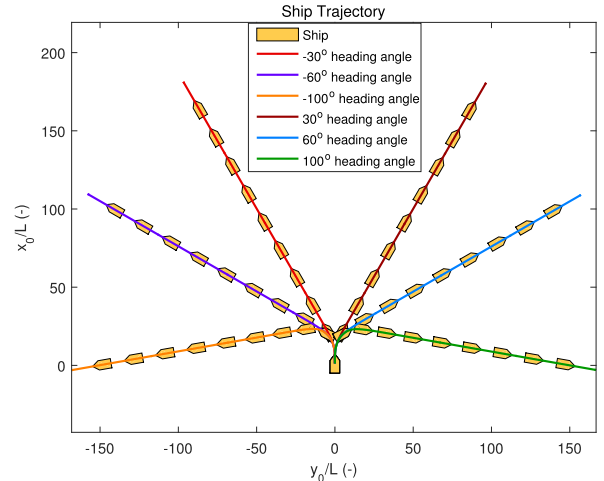
Values	Target heading angle angle					
	$-30°$	$-60°$	$-100°$	$30°$	$60°$	$100°$
K_P	8.28376	9.12158	9.80183	8.65684	9.67247	10.4912
K_I	0	0	0	0	0	0
K_D	42.4749	43.3403	43.1623	39.6816	41.1822	40.5429
MAD	1.2691	3.6868	8.638	1.2453	3.6459	8.6319
RMSE	5.3067	12.8524	25.1972	5.2856	12.8179	25.1796

(a) Ship trajectory.

(b) Ship tracking details.

FIGURE 10. Tracking different heading angles (AMBPS-PID, minimum MAD).

tracked as shown in Fig. 10 and Table 6. Fig. 10a shows the ship trajectories of different headings, and Fig. 10b shows the PID parameters, the tracking heading angle, search for the minimum error and the rudder angle change respectively.
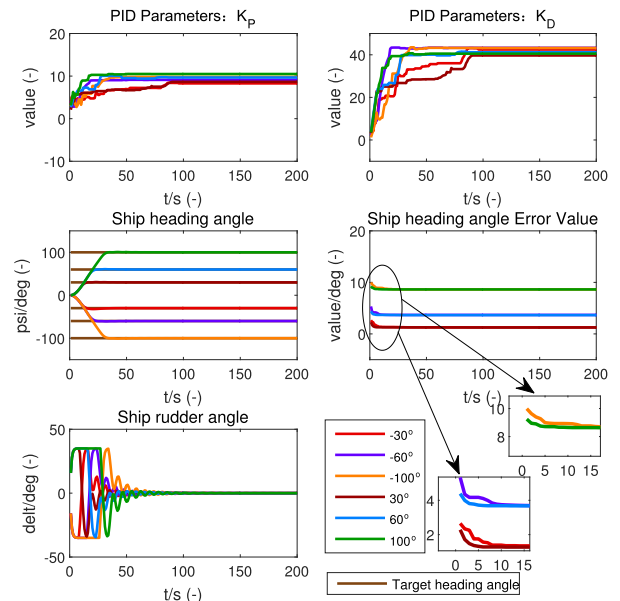
2) With RMSE optimum as the standard, the tracking error and the optimal PID parameters under different variable values are obtained as shown in Table 7.

Similarly, the optimum parameters are $n = 10, D_0 = 0.99, L_{step} = 1, Vm = 5$. the other angle can be tracked as shown in Fig. 11 and Table 8.

From Table 6 and Table 8, it can be concluded that the optimal PID parameters for tracking any heading angle are slightly different, basically fluctuate around $[K_P, K_I, K_D] = [10, 0, 40]$, both of MAD or RMSE. As can be seen from

Fig. 10 and Fig. 11, the current optimal control parameters can be obtained within 20 cycles. Moreover, the rudder adjustment frequency based on MAD optimization is low, so it is more suitable for ships with large inertia.

2) TRACKING TIME-VARYING HEADING ANGLES (ON-LINE CONTROLLER)

For time-varying heading, the AMBPS algorithm is used to adjust the PID parameters on-line for tracking. Based on the optimum parameters $n = 10, D_0 = 0.99, L_{step} = 1, Vm = 5$ obtained from Section V-C1, $\psi_{req} = 60 sin(0.01t)$ is taken as an example to simulate. Considering the efficiency problem, this paper takes $[Kp, Ki, Kd] = [10, 0, 40]$ as the initial value to adjust the PID parameters. Besides, adjusting parameters

TABLE 7. Tracking error and the optimal PID parameters under different variable values ($\psi_{req} = 60°$, minimum RMSE).

| n	K_P	K_I	K_D	RMSE	MAD
2	9.71417	0	36.1312	12.816	3.656
5	10.9873	0	41.4017	12.8159	3.6588
10	11.2468	0	42.4689	12.8158	3.6638
20	11.24	0	42.4375	12.8158	3.6641
30	11.2531	0	42.5009	12.8158	3.6641
D_0	K_P	K_I	K_D	RMSE	MAD
0.99	11.2468	0	42.4689	12.8158	3.6638
2	11.2227	0	42.3576	12.8158	3.6633
5	11.1357	0	41.8882	12.8159	3.662
10	11.2548	0	42.4935	12.8158	3.6641
20	11.2368	0	42.3228	12.8159	3.6642
L_{step}	K_P	K_I	K_D	RMSE	MAD
0.5	11.1871	0	42.2508	12.8159	3.6622
1	11.2468	0	42.4689	12.8158	3.6638
3	11.196	0	42.2384	12.8159	3.6627
5	11.232	0	42.3848	12.8158	3.6636
10	11.2556	0	42.5034	12.8158	3.6641
V	K_P	K_I	K_D	RMSE	MAD
0.5	7.77709	0	28.2573	12.8169	3.67
1	11.2422	0	42.4554	12.8158	3.6637
5	11.2468	0	42.4689	12.8158	3.6638
10	11.1951	0	42.2482	12.8158	3.6626
20	11.2621	0	42.5287	12.8158	3.6643

TABLE 8. Tracking different heading angle errors and PID parameters (AMBPS-PID, minimum RMSE).

PID parameters	Target heading angle					
	-30°	-60°	-100°	30°	60°	100°
K_P	9.01837	9.13704	10.7955	10.2119	11.2468	11.6113
K_I	0	0	0	0	0	0
K_D	44.6267	43.4239	45.0306	41.7029	42.4689	41.5925
RMSE	5.3023	12.7953	25.1966	5.2819	12.8158	25.1292
MAD	1.2923	3.9654	8.6615	1.2680	3.6641	8.648

TABLE 9. On-line adjustment steps and errors.

TS	MAD (standard)	RMSE	TS	RMSE	MAD (standard)
1	0.3922	0.4357	1	0.4357	0.3922
3	0.4436	0.5811	3	1.5418	0.6720
5	0.6170	0.8079	5	1.0553	0.6960
7	0.3978	0.4551	7	0.9059	0.6351
10	0.5448	0.8347	10	0.8789	0.5376
15	0.4011	0.4466	15	0.4438	0.3987
20	0.3828	0.4264	20	0.4233	0.3808
30	0.3719	0.4178	30	0.4175	0.3733
40	0.3609	0.4096	40	0.4105	0.3644
50	0.3522	0.4033	50	0.4043	0.3544
60	0.3464	0.4007	60	0.4027	0.3518
80	0.3483	0.4017	80	0.4031	0.3532
100	0.3489	0.4030	100	0.4015	0.3506
120	0.3337	0.3952	120	0.3969	0.3394
130	0.3240	0.3849	130	0.3894	0.3327
140	0.3269	0.3876	140	0.3897	0.3320
150	0.3277	0.3902	150	0.3963	0.3366
200	0.3853	0.4935	200	0.4864	0.3851
300	0.5062	0.6180	300	0.6121	0.5014
400	0.3945	0.4376	400	0.4353	0.3936
500	0.3974	0.4454	500	0.4367	0.3946
600	0.3856	0.4307	600	0.4343	0.3926
700	0.3592	0.4685	700	0.4680	0.3591

per step will also lead to inefficiency and may not be needed, so on-line adjustment can be divided into one-step adjustment and multi-steps adjustment. The PID parameters are adjusted at each TS step, and the error results are shown in Table 9.
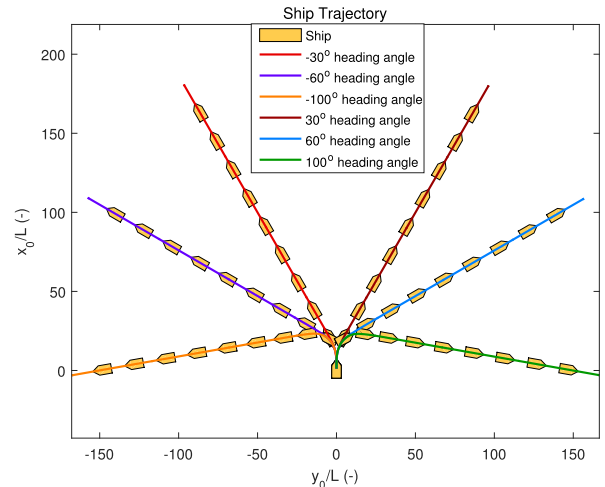
(a) Ship trajectory.
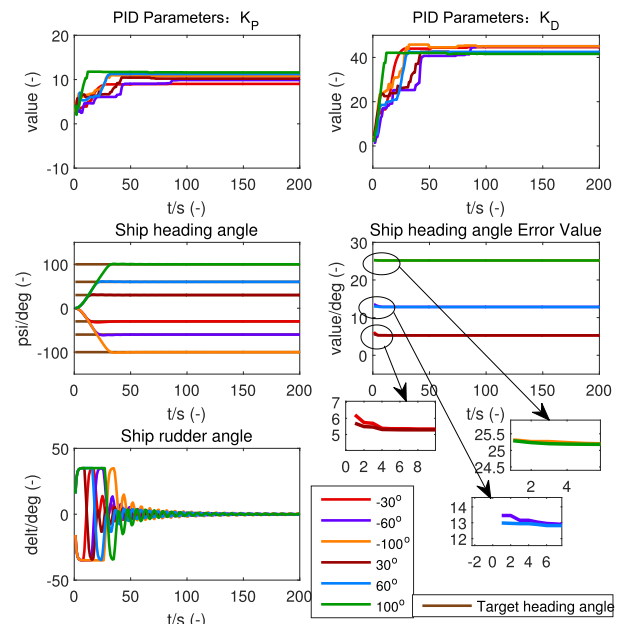
(b) Ship tracking details.

FIGURE 11. Tracking different heading angles (AMBPS-PID, minimum RMSE).

As can be seen from Table 9, whether minimum MAD or RMSE as the standard, the tracking result is the best when $TS = 130$. Similarly, the error results for tracking other time-varying heading angles are shown in Table 10, Fig. 12 and Fig. 13. Fig. 12a and Fig. 13a show the ship trajectories for different heading angles. Fig. 12b and Fig. 13b show the changes of PID parameters, the tracking heading angles, the minimum errors and the rudder angle, respectively.

3) PATH FOLLOWING SIMULATION RESULT

Path following control method adopts LOS navigation. Random path points are set for path following control. To make the tracking effect closer to the actual situation, and considering the site area, the simulation environment was selected
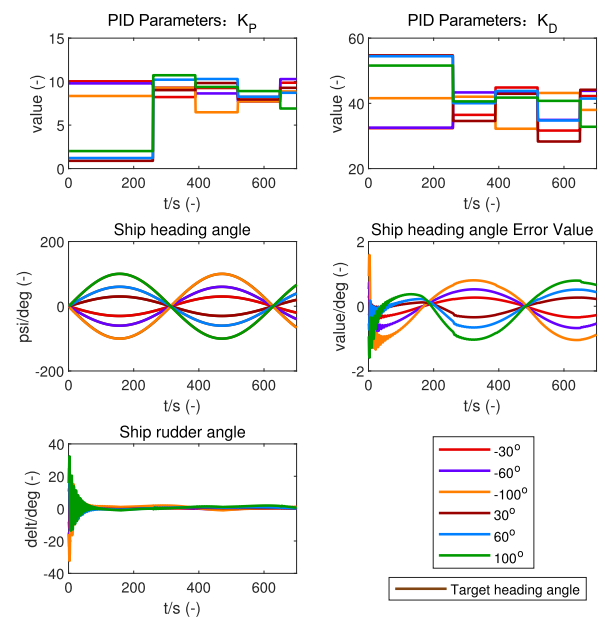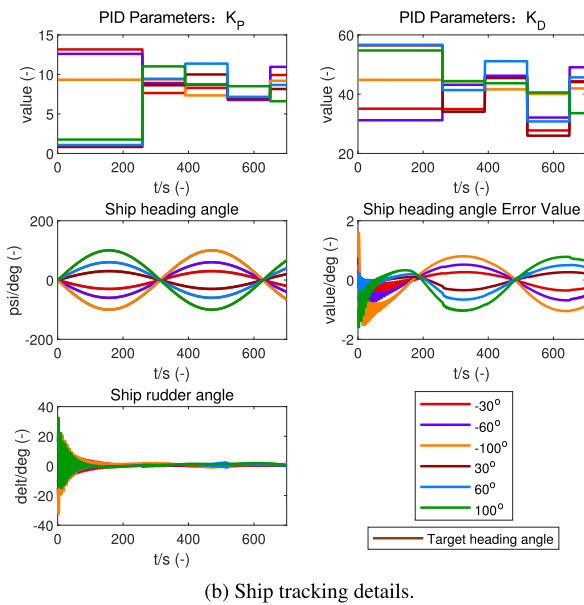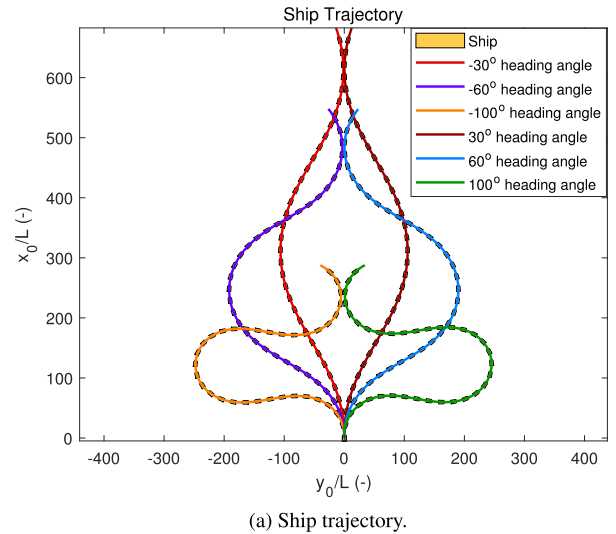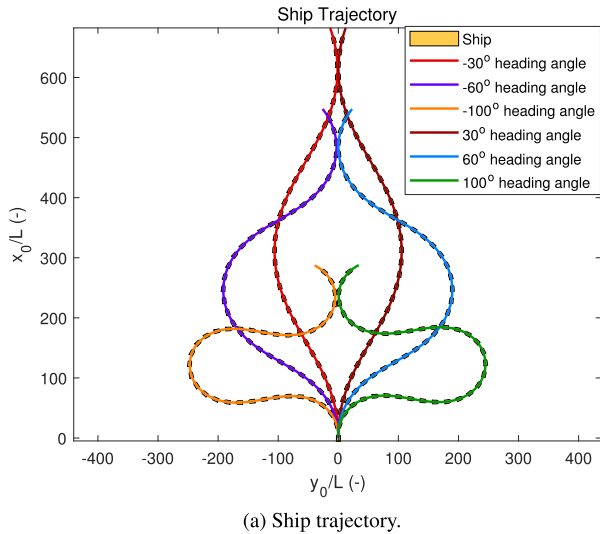
(a) Ship trajectory.

(b) Ship tracking details.

FIGURE 12. Tracking different time-varying heading angles (AMBPS-PID, minimum MAD).

TABLE 10. Tracking different time-varying heading angles errors ($\psi_{req} = A\sin(0.01t)$).

A	-30°	-60°	-100°	30°	60°	100°
MAD(standard)	0.2068	0.4055	0.6239	0.1650	0.3240	0.5413
RMSE	0.2383	0.4563	0.7059	0.1972	0.3849	0.6286
RMSE(standard)	0.2296	0.4506	0.7033	0.1986	0.3320	0.6319
MAD	0.2061	0.4053	0.6238	0.1679	0.3897	0.5503

from Kralingen Plas in Rotterdam, the Netherlands, as shown in Fig. 14a. Then set up the real target trajectory on Google Maps, as shown in Fig. 14b. Among them, path points include both clockwise and anticlockwise trajectories, which can fully reflect the path following effect. Based on Section V-C1 and Section V-C2, the optimal parameters of AMBPS-PID algorithm are shown in Table 11.

(a) Ship trajectory.

(b) Ship tracking details.

FIGURE 13. Tracking different time-varying heading angles (AMBPS-PID, minimum RMSE).

TABLE 11. Path following AMBPS-PID algorithm basic parameters.

Symbols	Value	Symbols	Value
$nStep$	2750	L_{step}	1
n	10	D_0	0.99
V_m	5	TS	130
K_P, K_I, K_D	10,0,40	$Titer$	10

Tracking the effect of manually adjusting the fixed parameter values $[K_P, K_I, K_D] = [5, 0, 20]$ is shown in Fig. 15. According to the on-line controller simulation analysis described in Section V-C2, it can be concluded that the heading angle tracking result is optimal when the $TS = 130$. Since the essence of LOS navigation is to track the heading angle,
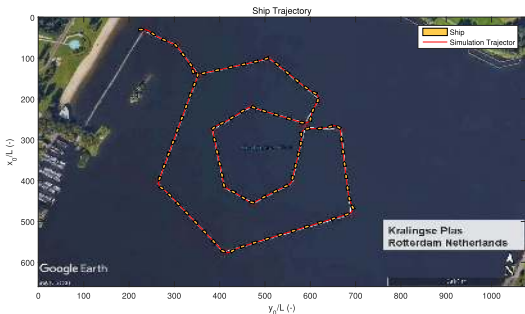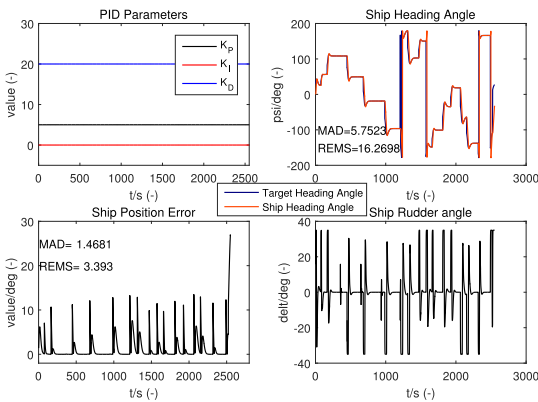
(a) Kralingen Plas map.
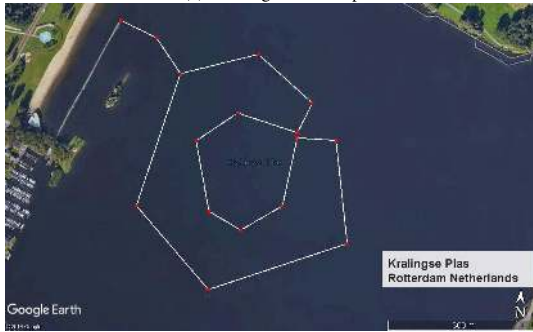
(b) Ship target trajectory map.

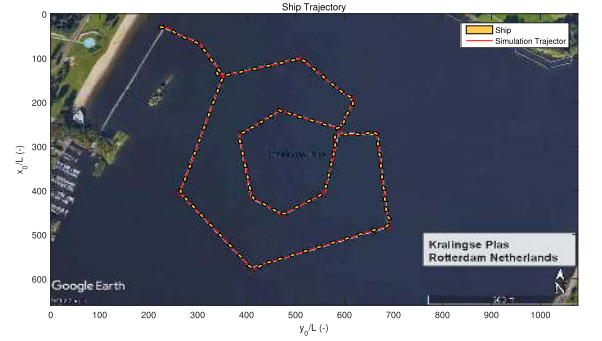**FIGURE 14.** Map of Kralingen Plas in Rotterdam, The Netherlands.
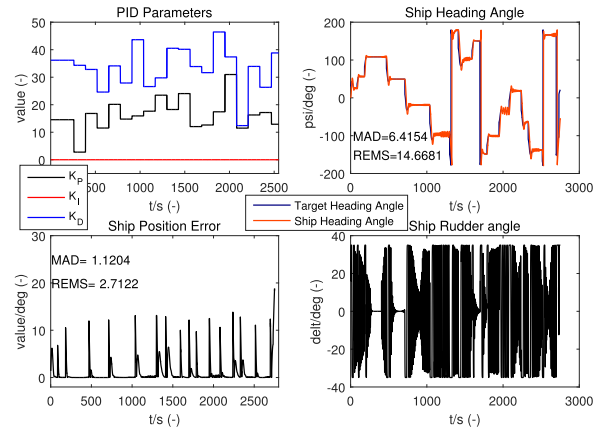

(a) Ship trajectory.

(b) Ship tracking details.

FIGURE 15. Path following effect with manually adjusting parameters.

the path following also selects the parameter adjustment once every 130 steps. The tracking effect is shown in Fig. 16. To verify the correctness of the $TS = 130$ analysis, the

(a) Ship trajectory.

(b) Ship tracking details.

FIGURE 16. Path following effect with AMBPS-PID adjusting parameters.

TABLE 12. Path following errors under different *TS*.

TS	1	10	50	100	130	150	200
MAD	1.6098	2.2984	1.7905	2.2082	1.1204	1.4716	1.4026
RMSE	4.3395	4.5441	4.5167	6.0054	2.7122	4.2046	4.168
TS	400	600	800	1000	1500	2000	2750
MAD	1.3488	1.3161	1.511	1.3865	1.4499	1.3691	1.3518
RMSE	4.199	4.1662	4.3273	4.2692	4.2476	4.2476	2.9221

tracking error results of different *TS* are given. The evaluation principle of tracking error is based on Eq. 23, and the results are shown in Table 12. From the results, it can be seen that the previous analysis is correct.

D. ANALYSIS AND COMPARISON OF RESULTS

1) RESULTS ANALYSIS

Section V-B and V-C describe the acquisition process of optimal parameters for adaptive motion control of 7m KVLCC2 ship. Through the Section V-B manual tuning, the simplest single heading angle is tested for preliminary judgment of parameter setting. For special case parameters, such as K_I in this paper, the parameter value can be determined quickly and the follow-up research can be simplified. Based on the roughly estimated PID parameters, the tracking MAD and RMSE of single heading angle and time-varying angles can be obtained. Although the emphasis of MAD and
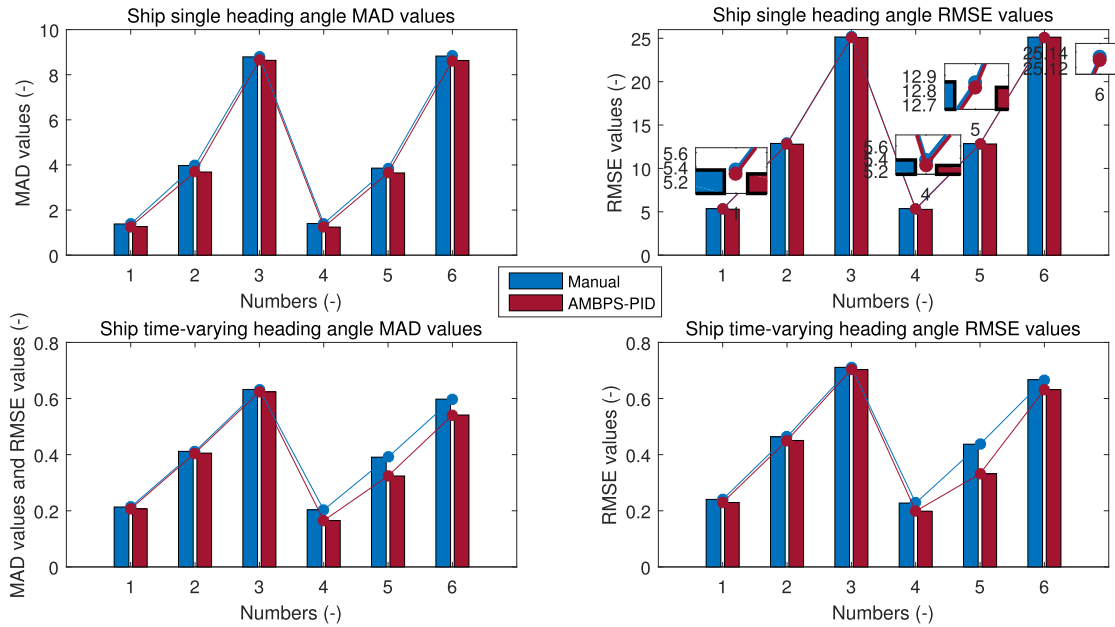
FIGURE 17. Tracking RMSE and MAD for ship control single heading angle and time-varying heading angles.
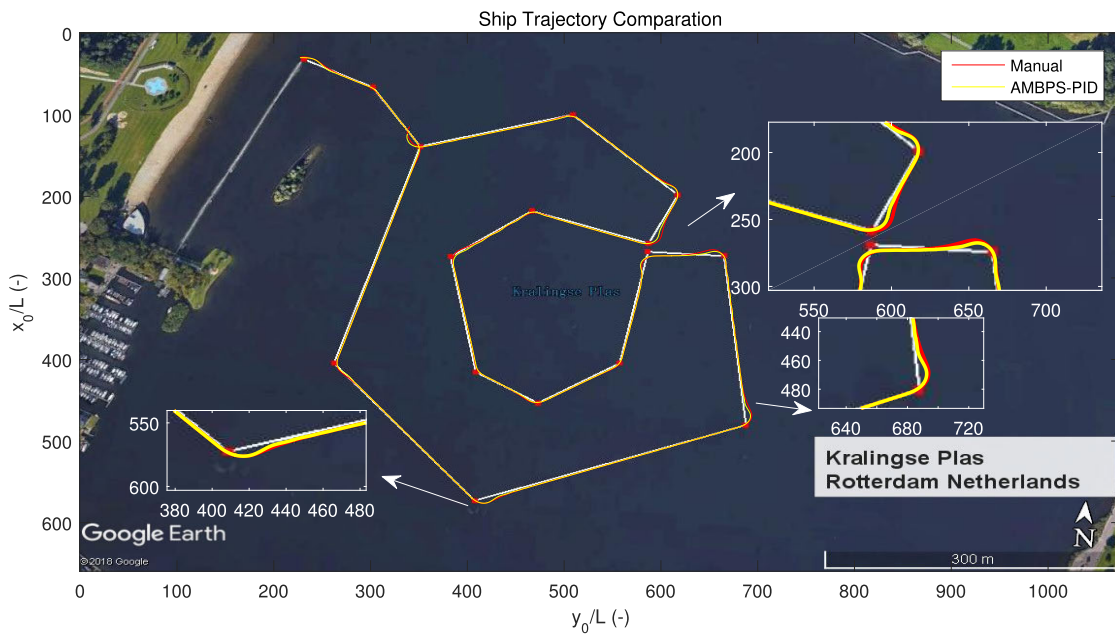

FIGURE 18. Comparison of manual setting parameters and AMBPS-PID online controller simulation results.

RMSE is different, the essence of MAD and RMSE is to reflect the errors between the calculated value and the target value, so the changing trend of the results is the same.

Section V-C shows how to search the optimal controller parameters step by step, from a single heading angle to time-varying heading angles. When applied to the 7m KVLCC2 ship, the influence of AMBPS algorithm parameters on control results is uncertain. To obtain the controller parameters suitable for this ship, optimal control parameters

of the AMBPS algorithm need to be first analyzed and obtained.

From Tables 5 and 7, it can be seen that the tracking error decreases with the increase of n, and does not change after $n \geq 10$. These results showed that the search range became wider with the increase of population individuals. In the case of satisfying the results, to ensure the search efficiency, the minimum value of n satisfying the conditions is selected. However, D_0 and L_{step} have little effect on tracking

TABLE 13. List of symbols.

KVLCC2 symbols			
a_H	Rudder force increase factor	r'	Non-dimensionalized yaw rate by $r L_{pp}/U$
B_{wl}	Beam at waterline	T	Propeller thrust
d	Ship draft	t_p	Thrust deduction factor
F_N	Rudder normal force	t_R	Steering resistance deduction factor
I_{zG}	Moment of inertia of ship around center of gravity	U	Resultant speed $(= \sqrt{u^2 + v_m^2})$
J_z	Added moment of inertia	u, v	Surge velocity, lateral velocity at center of gravity, respectively
L_{pp}	Ship length between perpendiculars	v_m	Lateral velocity at midship
m	Ship's mass	v_m'	Non-dimensionalized lateral velocity defined by v_m/U
m_x, m_y	Added masses of x axis direction and y axis direction, respectively	X_H, Y_H, N_H	Surge force, lateral force, yaw moment around midship acting on ship hull except added mass components
∇	Ship volume displacement	X_R, Y_R	Surge force, lateral force, yaw moment around
$o-xyz$	Ship fixed coordinate system taking the origin at midship	δ	Rudder angle
$o_0-x_0y_0z_0$	Space fixed coordinate system	ψ	Ship heading
r	Yaw rate	ρ	Water density
Controller symbols			
dl	Lateral error	δ_E	Rudder order
K_P, K_I, K_D	Proportional coefficient, integral coefficient and differential coefficient, respectively	ψ_{los}	LOS angle
R_{los}	LOS circle radius	ψ_{error}	heading error
t_{step}	Time step	ψ_{req}	Target heading angle
AMBPS algorithm symbols			
b_1, b_2	Step size coefficient, Antenna proportional coefficient	P_{best}	Individual best value of beetle
c_1, c_2	Position coefficients	r_1, r_2, P_{rand}	Random function in the range $[0, 1]$
D_0	Distance between the two antennas	$\tilde{X}_i$	Position of the beetle
G_{best}	Group best value of beetles	V	Velocity the beetle
L_{step}	Step size of beetle	ω	Inertia weight
N	Dimension	$\bar{f}(k)$	Normalized calibration factor
n	The number of beetles	$\Theta(k)$	Population fitness variance
$nStep$	The number of tracking step	$\tau(k)$	Aggregation degree of spatial position

(a) Rastrigrin function.

(b) Griewan function.

(c) Michalewicz function.

(d) Goldstein-Price function.

(e) Ackley function.

(f) Schaffer function.

FIGURE 19. Algorithms comparison results figure.

errors, which indicates that these two parameters have little effect on the results. Particle velocity determines the direction and distance of particle search, and the error decreases to the same level with the increase of V. Through this series of analyses, the optimal parameters of AMBPS are obtained, and the optimal parameters are the same whether it is MAD optimal or RMSE optimal.

After obtaining the optimal AMBPS parameters, the heading control is further developed from a single heading to time-varying heading angles, and an on-line controller is designed. On-line control needs to consider computational speed, which depends on the number of iterations and search frequency. The high search frequency will affect the actual navigation
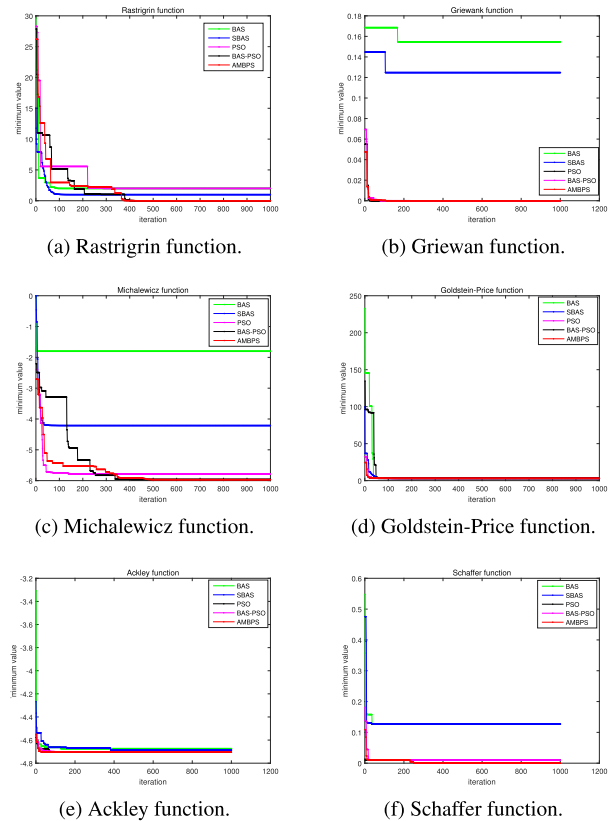
situation, and the low search frequency will affect the control accuracy. As shown in Fig. 10, 11 and Table 9, the optimal PID parameters can be obtained within 20 iterations and the search frequency being 130 times. The final path following control is implemented based on the optimal control parameters obtained above. To visualize the effects of the algorithm, compare the simulation results, as described in Section V-D2.

2) RESULTS COMPARISON

By summarizing the Tables 2, 3, 6, 8 and 10, we can get an intuitive comparison chart between manual and AMBPS-PID adaptive adjustment of PID parameters for tracking errors of single heading and time-varying headings, as shown in Fig. 17. From the comparison results, result errors of the AMBPS-PID algorithm are less than those of manual tuning. MAD is 0.19° and 0.03° lower on average, and RMSE is 0.05° and 0.03° lower on average.

Combining Fig. 15 and Fig. 16, it can get the simulation results in the comparison chart of path following, as shown in Fig. 18. From the enlarged part of Fig. 18, it can be seen that the tracking result of AMBPS-PID is better than that of traditional PID at larger turning points. MAD is 0.35 *m* lower and RMSE is 0.68 *m* lower, which is closer to the target path.

In summary, whether heading control or path following, the AMBPS-PID algorithm can achieve a better control effect. Because of the good control effect of the PID algorithm

TABLE 14. Test function list and results.

Test function	Average value of $Fitness_{best}$ (calculated 10 times)				
	BAS	SBAS	PSO	BAS-PSO	AMBPS
$F_1(x) = \sum_{j=1}^{n}(x_i^2 - 10cos(2\pi x_i) + 10), |x_i| \leq 5.12$	5.366108	2.387898	1.16078	0.73911	0
$F_2(x) = \frac{1}{4000}\sum_{i=1}^{n}x_i^2 - \prod_{i=1}^{n}cos(\frac{x_i}{\sqrt{i}}) + 1, |x_i| \leq 600$	0.132618	0.134561	0	0	0
$F_3(x) = \sum_{i=1}^{d}sin(x_i)[sin(\frac{ix_i^2}{\pi})]^2 m, m = 10, d = 5, 0 \geq x_i \leq 10$	-2.19876	-5.15766	-5.76857	-5.85693	-5.92595
$F_4(x) = [1 + (x_1 + x_2 + 1)^2(19 - 14x_1 + 3x_1^2 - 14x_2 + 6x_1x_2 + 3x_2^2)][30 + (2x_1 - 3x_2)^2(18 - 32x_1 + 12x_1^2 + 48x_2 - 30x_1x_2 + 27x_2^2)]$	3.00355	3	3	3	3
$F_5(x) = -20exp(-0.2\sqrt{\frac{1}{n}\sum_{i=1}^{n}x_1^2}) - exp(\frac{1}{n}\sum_{i=1}^{n}cos(2\pi x_i)) + 20 + e, |x_i| \leq 1$	-4.67959	-4.67563	-4.70256	-4.7056	-4.7056
$F_6(x) = 0.5 + \frac{(sin\sqrt{x_1^2 + x_2^2}) - 0.5}{(1 + 0.001(x_1^2 + x_2^2))^2}, -10 \geq x_1, x_2 \leq 10$	0.1234457	0.1127442	0.002915	0.003886	0.0009716

itself, the advantage of the AMBPS-PID algorithm is mainly reflected in these two aspects:

1) It does not need to recalculate the optimal PID parameters when tracking different heading angles, so it is adaptive.
2) The error is significantly reduced at the larger turning points.

VI. SUMMARY

In this research, the AMBPS-PID algorithm is used to study the adaptive motion control of ships, and the heading and path following controller are designed. Based on the simulation analysis, the conclusions of this paper are as follows:

1) The rudder turning rate control is introduced into the motion controller, which makes the control results more in line with the actual ship situation.
2) This paper combines BAS with the PSO algorithm and introduces an adaptive mutation operator. Based on this, the AMBPS algorithm is developed, and the fast search of PID optimal parameters is successfully realized.
3) AMBPS algorithm can optimize the parameters of PID with fewer iterations, which shows that the efficiency of this algorithm is better.
4) By choosing the best frequency of variation through simulation analysis, the adaptability and efficiency of the algorithm can be further realized, which has a certain significance for actual navigation.
5) Whether heading control or path following, simulation results show that the error of the AMBPS-PID algorithm is smaller than that of traditional PID (whether MAD or RMSE). Among them, the most obvious advantage is at the larger turning points of path following.

In the future, this algorithm can be applied to the actual navigation test results. AMBPS algorithm itself can be further improved. Other algorithms can also be combined with the AMBPS algorithm to study ship motion control.

APPENDIXES
APPENDIX A
SYMBOLS
List of symbols is shown as Table 13.

APPENDIX B
TEST FUNCTION LIST AND COMPARING RESULTS OF ALGORITHMS
Test function list and comparing results of algorithms are shown as Table 14 and Fig. 19.

REFERENCES
[1] X. L. Zhang and X. L. Jia, *Ship Motion Control* Beijing, China: National Defense Industry Press, 2006.
[2] M. H. Moradi and M. R. Katebi, "Predictive PID control for ship autopilot design," *IFAC Proc.*, vol. 34, no. 7, pp. 375–380, Jul. 2001.
[3] J. Malecki, "Applying of fuzzy logic to precise control of the ship motion," in *Proc. 2nd IEEE Int. Conf. Math. Comput. Sci. Ind.*, Aug. 2015, pp. 125–130.
[4] Y. A. Ahmed and K. Hasegawa, "Fuzzy reasoned Waypoint controller for automatic ship guidance," *IFAC Papers Online*, vol. 49, no. 23, pp. 604–609, Sep. 2016.
[5] M. Tomera, "Ant colony optimization algorithm applied to ship steering control," *Procedia Comput. Sci.*, vol. 35, pp. 83–92, Sep. 2014.
[6] G. Y. Liu, Y. B. Hou, Y. Luo, and D. Li, "Genetic algorithm application for optimization of PID parameters in dynamic positioning vessel," *MATEC Web Conf.*, vol. 139, p. 153, Dec. 2017.
[7] J. M. Larrazabal and M. S. Peñas, "Intelligent rudder control of an unmanned surface vessel," *Expert Syst. Appl.*, vol. 55, pp. 106–117, Aug. 2016.
[8] G. Y. Li, "Research on particle swarm optimized fractional-order controller and its application to control for underactuated surface vessels," Ph.D. dissertation, Dept. Traffic Inf. Eng. Control, Dalian Maritime Univ., Dalian, China, 2016.
[9] M. C. Fang, Y. Z. Zhuo, and Z. Y. Lee, "The application of the self-tuning neural network PID controller on the ship roll reduction in random waves," *Ocean Eng.*, vol. 37, no. 7, pp. 529–538, May 2010.
[10] V. L. Tran and N. Im, "A study on ship automatic berthing with assistance of auxiliary devices," *Int. J. Naval Archit. Ocean Eng.*, vol. 4, no. 3, pp. 199–210, Sep. 2012.
[11] Y. A. Ahmed and K. Hasegawa, "Automatic ship berthing using artificial neural network based on virtual window concept in wind condition," *IFAC Proc.*, vol. vol., 45, no. 24, pp. 286–291, Sep. 2012.
[12] Y. A. Ahmed and K. Hasegawa, "Artificial neural network based automatic ship berthing combining PD controlled side thrusters—A combined controller for final approaching to berth," in *Proc. IEEE 13th Int. Conf. Control Autom. Robot. Vis.*, Dec. 2015, pp. 1304–1309.

[13] Z. Dong, T. Bao, M. Zheng, X. Yang, L. Song, and Y. Mao, "Heading control of unmanned marine vehicles based on an improved robust adaptive fuzzy neural network control algorithm," *IEEE Access*, vol. 7, pp. 9704–9713, 2019.

[14] X. Y. Jiang and S. Li, "BAS: Beetle antennae search algorithm for optimization problems," Oct. 2017, *arXiv:1710.10724*. [Online]. Available: https://arxiv.org/abs/1710.10724

[15] J. Y. Wang, and H. X. Chen, "BSAS: Beetle swarm antennae search algorithm for optimization problems," Jul. 2018, *arXiv:1807.10470*. [Online]. Available: https://arxiv.org/abs/1807.10470

[16] M. J. Lin and Q. H. Li, "A hybrid optimization method of beetle antennae search algorithm and particle swarm optimization," *DEStech Trans. Eng. Technol. Res.*, vol. 1, pp. 396–401, Sep. 2018.

[17] T. Wang, L. Yang, and Q. Liu, "Beetle swarm optimization algorithm: Theory and application," Aug. 2018, *arXiv:1808.00206*. [Online]. Available: https://arxiv.org/abs/1808.00206

[18] S. Mohammadafzali, "A mathematical model for the maneuvering simulation of a propelled SPAR vessel," Ph.D. dissertation, Faculty Eng. Appl. Sci., Memorial Univ. Newfoundland, Newfoundland, JL, Canada, 2016.

[19] J. Kennedy, "Particle swarm optimization," *Encyclopedia Mach. Learn.*, vol. 10, pp. 760–766, Nov. 2010.

[20] T. I. Fossen, K. Y. Pettersen, and R. Galeazzi, "Line-of-sight path following for Dubins paths with adaptive sideslip compensation of drift forces," *IEEE Trans. Control Syst. Technol.*, vol. 23, no. 2, pp. 820–827, Mar. 2015.

[21] H. Yasukawa and Y. Yoshimura, "Introduction of MMG standard method for ship maneuvering predictions," *J. Marine Sci. Technol.*, vol. 20, no. 1, pp. 37–52, Mar. 2015.

JIALUN LIU was born in Fushun, Liaoning, China, in 1987. He received the M.S. degree in traffic information engineering and control from the Wuhan University of Technology, Wuhan, China, in 2013, and the Ph.D. degree in ship design, production and operation from the Delft University of Technology, Delft, The Netherlands, in 2017. He is currently an Associate Professor with the Intelligent Transportation Systems Research Center, Wuhan University of Technology. His research interests include the motion control of smart ships, (inland) ship maneuverability, and functional testing of smart ships.

LE WANG was born in Shijiazhuang, Hebei, China, in 1990. She received the B.S. and M.S. degrees in mechanical engineering from the Wuhan University of Technology, Wuhan, China, in 2014 and 2017, respectively. She is currently pursuing the Ph.D. degree. Her research interests include mechanical and logistics engineering, intelligent ship control, and optimization algorithm.

SHIJIE LI was born in Jingmen, Hubei, China, in 1988. She received the M.S. degree in control theory and engineering from Harbin Engineering University, Harbin, China, in 2013, and the Ph.D. degree in transport engineering and logistics from the Delft University of Technology, Delft, The Netherlands, in 2016. Her research interests include the collaborative optimization of logistics systems, ship motion control, and multiship system operation optimization.

QING WU was born in Anhua, Hunan, China, in 1962. She received the M.S. degree in mechanical engineering from the Wuhan University of Technology, Wuhan, China, in 1997. Since 2005, she has been a Professor and a Ph.D. Supervisor with the Department of Logistics Automation, School of Logistics Engineering, Wuhan University of Technology. She holds and participates in more than 30 projects. Her research interest includes water traffic safety and information.

RUDY R. NEGENBORN received the Ph.D. degree from the Delft University of Technology, Delft, The Netherlands, in 2007. He is currently a Full Professor of multimachine operations and logistics (full-time, fixed-term), the Head of section transport engineering and logistics, and the Director of studies MSC transport, infrastructure, and logistics. He is the author of four books and more than one hundred articles. His research interests include logistics engineering and ship motion control.

● ● ●